AMERICAN SOCIETY FOR MICROBIOLOGY | Journal of Bacteriology®

RESEARCH ARTICLE

In Situ Structures of Polar and Lateral Flagella Revealed by Cryo-Electron Tomography

Shiwei Zhu,[a,b] Maren Schniederberend,[c] Daniel Zhitnitsky,[c] Ruchi Jain,[c] Jorge E. Galán,[a] Barbara I. Kazmierczak,[a,c] Jun Liu[a,b]

[a]Department of Microbial Pathogenesis, Yale University School of Medicine, New Haven, Connecticut, USA
[b]Microbial Sciences Institute, Yale University, West Haven, Connecticut, USA
[c]Department of Medicine (Infectious Diseases), Yale University School of Medicine, New Haven, Connecticut, USA

ABSTRACT The bacterial flagellum is a sophisticated self-assembling nanomachine responsible for motility in many bacterial pathogens, including *Pseudomonas aeruginosa*, *Vibrio* spp., and *Salmonella enterica*. The bacterial flagellum has been studied extensively in the model systems *Escherichia coli* and *Salmonella enterica* serovar Typhimurium, yet the range of variation in flagellar structure and assembly remains incompletely understood. Here, we used cryo-electron tomography and subtomogram averaging to determine *in situ* structures of polar flagella in *P. aeruginosa* and peritrichous flagella in *S.* Typhimurium, revealing notable differences between these two flagellar systems. Furthermore, we observed flagellar outer membrane complexes as well as many incomplete flagellar subassemblies, which provide additional insight into mechanisms underlying flagellar assembly and loss in both *P. aeruginosa* and *S.* Typhimurium.

IMPORTANCE The bacterial flagellum has evolved as one of the most sophisticated self-assembled molecular machines, which confers locomotion and is often associated with virulence of bacterial pathogens. Variation in species-specific features of the flagellum, as well as in flagellar number and placement, results in structurally distinct flagella that appear to be adapted to the specific environments that bacteria encounter. Here, we used cutting-edge imaging techniques to determine high-resolution *in situ* structures of polar flagella in *Pseudomonas aeruginosa* and peritrichous flagella in *Salmonella enterica* serovar Typhimurium, demonstrating substantial variation between flagella in these organisms. Importantly, we observed novel flagellar subassemblies and provided additional insight into the structural basis of flagellar assembly and loss in both *P. aeruginosa* and *S.* Typhimurium.

KEYWORDS bacterial cell motility, bacterial envelope, flagellar assembly, nanomachine, protein export, type III secretion

The bacterial flagellum is a complex, multiprotein nanomachine that allows bacteria to swim in liquid environments. Flagella from different species contain structurally conserved components. The cytoplasmic C-ring, which integrates chemotaxis signals, abuts the inner membrane MS-ring and interacts with stator proteins that anchor in the peptidoglycan and transform chemical energy into flagellar rotation (1). A dedicated flagellar export apparatus secretes proteins that assemble into the rod, hook, and filament to form the rotating axial "propeller" (2). L- and P-rings in the outer membrane and peptidoglycan, respectively, serve as a "bushing" for the flagellar rod as it traverses the cell envelope (3, 4).

Variation in specific features of the flagellum, as well as in flagellar number and placement, results in structurally distinct flagella that appear to be adapted to the specific environments that bacteria encounter (5–7). *Escherichia coli* and *Salmonella enterica* serovar Typhimurium assemble several external flagella at locations all over the

Citation Zhu S, Schniederberend M, Zhitnitsky D, Jain R, Galán JE, Kazmierczak BI, Liu J. 2019. *In situ* structures of polar and lateral flagella revealed by cryo-electron tomography. J Bacteriol 201:e00117-19. https://doi.org/10.1128/JB.00117-19.

Editor Ann M. Stock, Rutgers University-Robert Wood Johnson Medical School

Address correspondence to Barbara I. Kazmierczak, barbara.kazmierczak@yale.edu, or Jun Liu, jliu@yale.edu.

M.S. and D.Z. contributed equally to this work.

Received 7 February 2019
Accepted 16 April 2019
Accepted manuscript posted online 22 April 2019
Published 10 June 2019

cell (i.e., peritrichous). The counterclockwise rotation of these filaments causes them to form a bundle that powers a bacterial "run" toward a chemoattractant, while clockwise rotation results in filament unbundling and a reorienting bacterial "tumble" (8). Other bacteria restrict flagellar assembly to polar sites, among them *Vibrio* spp., which assemble one flagellum at a single pole; *Campylobacter jejuni*, with one flagellum at each pole; and *Helicobacter pylori*, with several flagella at one pole. Some bacteria, such as *Vibrio parahaemolyticus* and *Vibrio alginolyticus*, separately carry both lateral and polar flagellar systems (9). These marine *Vibrio* spp. also express two sets of stator proteins that use Na^+ or H^+ gradients to power rotation of the polar versus lateral flagella, respectively, in different environments (10, 11). The filament can even be assembled internally, as is the case for spirochetes that assemble periplasmic flagella between their cytoplasmic and outer membranes (12). This variety of flagellar structures, number, position, and regulation are reflected in the genetic loci that encode flagellar structural genes and regulators, which show clear evidence of evolution and diversification across bacterial phyla (13, 14). Cryo-electron tomography (cryo-ET) studies have revealed a corresponding variation in the macromolecular structures of the flagellar motor (5, 6). It is proposed that some of these unique structural features are related to the amount of torque the flagellum can generate or to its ability to interact with H^+-versus Na^+-driven stator systems (15, 16).

The opportunistic human pathogen *Pseudomonas aeruginosa* assembles a single polar flagellum that powers a run-and-reverse form of motility similar to that described for *Vibrio* spp. (17, 18). Although core structural features of the flagellum are well conserved and flagellar gene expression is regulated in similar stepwise fashions in *P. aeruginosa* and *E. coli* (19, 20), the *P. aeruginosa* flagellum appears to have several unusual features. Two distinct stators can drive rotation of the flagellum, and in contrast to *V. alginolyticus*, both appear to use proton motive force to generate torque (21). One of these stators can support swarming of monotrichous *P. aeruginosa* through media of increased viscosity (21, 22), in contrast to *V. parahaemolyticus*, which induces the expression of multiple lateral flagella in order to swarm (9). The *P. aeruginosa* flagellum propels bacteria in liquid media in response to signals sensed by more than 26 chemoreceptors (23). However, the flagellum also mediates bacterial attachment to surfaces (24) and initiates the process leading to biofilm formation (25). Despite the central importance of the flagellum in *P. aeruginosa* biology, a detailed structure of this nanomachine is not available.

We applied cryo-ET to visualize the *P. aeruginosa* polar flagellum *in situ* at high resolution and observed structural features that distinguish this flagellum from that of the model organism *S.* Typhimurium. We also observed "incomplete" flagellar assemblies in both *P. aeruginosa* and *S.* Typhimurium and investigated their possible roles in flagellar assembly and/or loss.

RESULTS

***In situ* structure of the intact *P. aeruginosa* flagellar motor and "incomplete" assemblies.** We used cryo-ET to visualize the single flagellum located at the pole of wild-type (WT) *P. aeruginosa* cells. Its basal body substructures, as well as the inner membrane, peptidoglycan layer, and outer membrane, were well defined in the tomograms (Fig. 1). In addition, we observed structures suggestive of "incomplete" flagellar assemblies at a subset of cell poles. These included the following: a flagellum lacking the hook and filament (Fig. 1D and H); a flagellum lacking the rod, hook, and filament (Fig. 1E and I); and an outer membrane complex without associated MS- or C-rings (Fig. 1F and J). Although these structures were much less common than complete flagellar motors in WT bacteria, the number of these "incomplete" assemblies increased in the hyperflagellated Δ*fleN* mutant (see below).

To determine the *in situ* structures of the *P. aeruginosa* flagellar motor at higher resolution, we made use of a hyperflagellated mutant, the Δ*fleN* mutant, which lacks the FleN/FlhG protein required for restriction of polar flagellar number in *P. aeruginosa*, *Vibrio* spp., and *Shewanella* spp. (26–30). This allowed us to visualize 1,170 flagellar

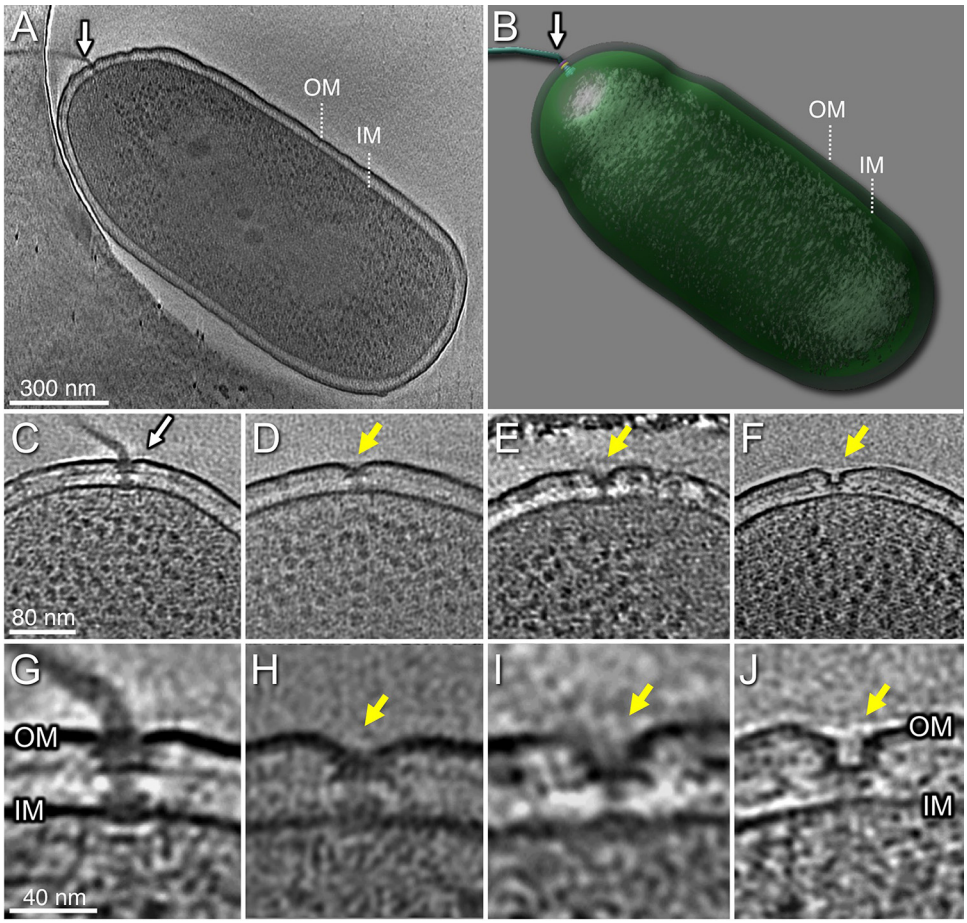

FIG 1 Tomograms of *P. aeruginosa* PAK cells show the intact polar flagellum and subcomplexes. (A) One slice from a whole-cell tomogram shows a single polar flagellum. (B) A surface rendering of the tomogram shown in panel A. (C) A slice from one tomogram shows the intact flagellar motor. (D) A slice from one tomogram shows a flagellum lacking the hook and filament. (E) A tomogram slice shows a flagellum without the rod, hook, and filament. (F) A tomogram slice shows a novel structure with a large pore in outer membrane (OM). (G) A zoomed-in view of the flagellar motor shows major components embedded in OM and inner membrane (IM). (H) A zoomed-in view of the motor in panel D. (I) A zoomed-in view of the motor in panel E. (J) A zoomed-in view of the outer membrane pore in panel F.

motors and determine an *in situ* structure at higher resolution by subtomogram averaging (Fig. 2). A comparison of the *P. aeruginosa* flagellar motor structure with those of *S.* Typhimurium and *V. alginolyticus* (see Fig. S1 in the supplemental material) identified features common to all of these motors, namely the MS-ring, C-ring, export apparatus, rod, and P- and L-rings (Fig. 2C and E; see Fig. S2 in the supplemental material). The polar flagellar motors of *P. aeruginosa* and *V. alginolyticus* shared additional features not seen in the *S.* Typhimurium structure. Prominent densities adjacent to the P- and L-rings were observed in the *P. aeruginosa* flagellar motor, occupying a similar location to the T- and H-rings of the *V. alginolyticus* structure (31).

The *Vibrio* T-ring is composed of two proteins, MotY and MotX, while FlgT is a component of the H-ring (31–33). Homologs of MotX and FlgT are not identified in *P. aeruginosa*, but a MotY (PA3526) homolog is encoded (21). We constructed the deletion mutant Δ*motY* in *P. aeruginosa* and used cryo-ET and subtomogram averaging to determine its motor structure. The density adjacent to the P-ring was not visible in Δ*motY* (see Fig. S3 in the supplemental material), suggesting that MotY contributes to the assembly of a "T-ring"-like structure in *P. aeruginosa*. Further work is required to determine if any proteins in addition to MotY participate in the formation of this ring and to identify proteins that contribute to the densities that are seen adjacent to the L-ring.

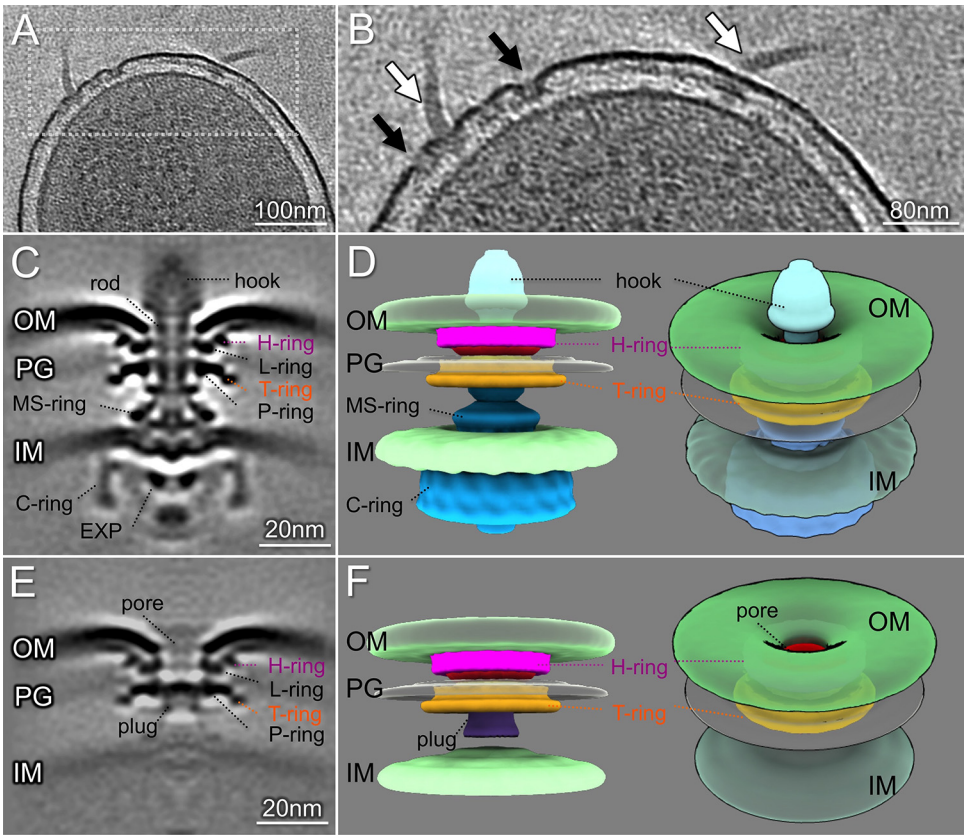

FIG 2 Structures of the *P. aeruginosa* flagellar motor and subassembly. (A) A representative slice of a cell pole reconstruction from *P. aeruginosa* Δ*fleN* showing multiple flagella. (B) A zoomed-in view of the slice shown in panel A. Flagellar motors and hooks are indicated by white arrows. The flagellar outer membrane complexes (FOMCs) are shown by black arrows. (C) A slice of an averaged structure of the intact flagellar motor. Note the striking curvature of the outer membrane. (D) Side and tilted views of the three-dimensional (3D) surface rendering of the motor show the curvature of the outer membrane and the FOMC. (E) A slice of an averaged structure of the FOMC. (F) A 3D surface rendering of the FOMC. The novel "plug" is colored purple. A tilted view of the 3D surface rendering shows the membrane pore in the FOMC. EXP, export apparatus; OM, outer membrane; PG, peptidoglycan layer; IM, inner membrane.

The interface between the flagellar motor and outer membrane in *P. aeruginosa* differed markedly from that seen in either *S.* Typhimurium or *V. alginolyticus* (Fig. S1). Compared with *S.* Typhimurium, the *P. aeruginosa* outer membrane appeared to undergo significant deflection at its interface with the L-ring (Fig. 2C; Fig. S1A). Although the spacing between the inner and outer membranes of *S.* Typhimurium and *P. aeruginosa* was quite similar (~33 nm), the distance between the L-ring and the inner membrane was 24.6 nm in *P. aeruginosa*, much less than that observed for the motors of *S.* Typhimurium and *V. alginolyticus* (~29.1 nm) (Fig. S1). Thus, the *P. aeruginosa* motor is both shorter and wider than that of *S.* Typhimurium.

***In situ* structure of a flagellar outer membrane complex in *P. aeruginosa*.** The cell poles of Δ*fleN* bacteria contained multiple intact flagellar motors, as well as numerous examples of a flagellar outer membrane complex (FOMC) (Fig. 2A and B) that was rarely observed in WT cells (Fig. 1F and J; Table 1). Subtomogram averaging of these abundant FOMCs allowed us to determine the FOMC *in situ* structure at high resolution (Fig. 2C and E). The FOMCs closely resembled the outer membrane portion of the fully assembled flagellar motor, possessing both P/L-rings and the adjacent T- and H-ring-like densities (Fig. 2C, D, F, and G; see Fig. S4 in the supplemental material). The outer membrane again exhibited significant deflection at its interface with the FOMC L-ring (Fig. 2), suggesting that this deformation was due to outer membrane interactions with the L/H-ring alone. The FOMC formed a large outer membrane pore

TABLE 1 Cryo-ET data and analysis

Sample name	Microscope	No. of tomograms	No. of subtomograms	No. of motors	No. of FOMCs	No. of intermediates
PAK (WT)	Titan Krios	217	112	103	6	3
PAK Δ*fleN*	Polara	340	1,746	1,170	566	11
PAK Δ*fleN* Δ*flgG*	Titan Krios	46	121	121	0	0
PAK Δ*flgG*	Titan Krios	193	42	42	0	0
PAK Δ*motY*	Titan Krios	65	26	26	0	0
S. Typhimurium SB1780	Polara	1,470	3,695	3,669	6	20

of ~12 nm in diameter and had a plug-like density within the P-ring, whereas the rod occupied this axial region in the flagellar motor (Fig. 2C, F, and H). Lastly, the inner membrane and MS-ring were clearly resolved in the intact motor structure, while the MS-ring was absent and the inner membrane poorly resolved in the structure of the FOMC. Classification of FOMC structures and averaging of these subgroups allowed us to observe variation in the distance between the outer membrane surrounding the FOMC and the inner membrane (see Fig. S5 in the supplemental material). In contrast, the distance between the inner and outer membranes in the vicinity of intact flagellar motors was less variable (Fig. S5), consistent with the notion that flagellar rod length is tightly controlled (34).

FOMCs as well as intact flagellar motors are observed in *S.* Typhimurium. Our examination of *P. aeruginosa* revealed FOMCs composed of L/P- and T/H-rings forming plugged pores in the outer membrane, as well as "incomplete" flagellar assemblies (Fig. 1). To determine whether FOMCs were restricted to bacteria with polar flagella, we examined minicells prepared from peritrichously flagellated *S.* Typhimurium bacteria. We observed many fully assembled flagellar motors (Fig. 3A) and determined their structure with sufficient detail to resolve the well-ordered bilayers of both the inner and outer membranes and the close apposition of the L-ring to both the inner and outer leaflets of the outer membrane (Fig. 3D). After screening tomograms of 1,470 *S.* Typhimurium minicells (Table 1), we identified six FOMCs and determined their low-resolution structure (Fig. 3B and C). The overall shape and dimensions of the *S.* Typhimurium FOMC were well matched to those of the L/P rings of the fully assembled flagellar motor (Fig. 3E and H). As in *P. aeruginosa*, the *S.* Typhimurium FOMC formed a pore of approximately 12 nm, with a plug-like density visible below the P-ring. This membrane pore would be large enough to accommodate the rod assembly, as shown in the fully assembled flagellar motor (Fig. 3D and G).

Subtomogram classification was used to analyze over 3,600 *S.* Typhimurium flagellar assemblies. Most class averages showed fully assembled motors, but others revealed "incomplete" assemblies. In addition to the class containing the six FOMCs, we observed a class with 20 particles that clearly differed from either the intact motor or the FOMC (Fig. 3F and I). In this class, a FOMC appeared axially aligned with a MS/C-ring structure in the absence of a rod density (Fig. 3F and I), raising the question of whether the FOMC can assemble independently of the rod and provide a conduit through which the rod reaches the outer membrane (Fig. 3F and I).

The FOMC is not observed in *P. aeruginosa* mutants lacking the distal rod protein FlgG. To test whether the FOMC represents a flagellar assembly intermediate that can form in the absence of the flagellar rod, we constructed an in-frame, unmarked deletion of the gene encoding the predicted distal rod protein *flgG* in the PAK and PAK Δ*fleN* backgrounds. PAK Δ*flgG* was nonmotile in soft-agar swimming assays, but motility was fully complemented by expression of plasmid-encoded FlgG (see Fig. S6 in the supplemental material). Cryo-ET reconstructions from both PAK Δ*flgG* and PAK Δ*fleN* Δ*flgG* cells showed flagellar subcomplexes corresponding to the MS-ring and C-ring (Fig. 4). In 193 PAK Δ*flgG* cell pole tomograms, we observed 42 MS/C-ring complexes but no FOMC (Table 1). Likewise, we observed 121 MS/C-ring complexes from 46 PAK Δ*fleN* Δ*flgG* cell pole tomograms but no FOMC (Fig. 4B and C). The averaged structure of these complexes clearly shows the C-ring, MS-ring, and proximal rod, while the distal rod is absent (Fig. 4D and E). These results strongly

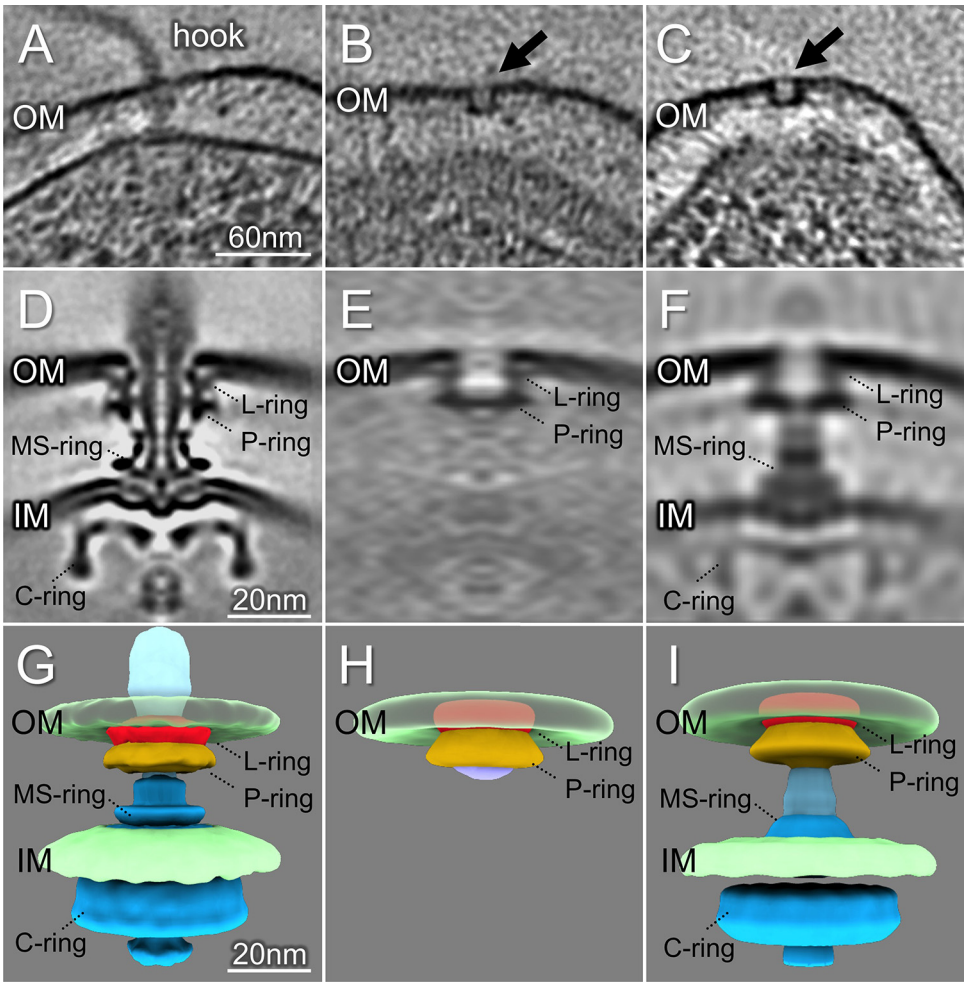

FIG 3 Intact flagellar motor, FOMC, and a subcomplex revealed in *S.* Typhimurium minicells. (A) A representative tomogram slice of an *S.* Typhimurium minicell shows a complete flagellar motor. (B, C) Two representative slices show FOMCs in *S.* Typhimurium. (D) A slice of a subtomogram average of the complete *S.* Typhimurium flagellar motor. (E) A slice of the averaged structure of the FOMC. (F) One class average shows the FOMC assembly aligned with the MS-ring in the absence of a distal rod. (G) Surface view of the intact flagellar motor. (H) A 3D surface rendering of the FOMC structure. (I) Surface rendering of a subcomplex in which the MS-ring is associated with the FOMC.

argue that the FOMC cannot form in the absence of the distal rod protein, in agreement with previous models which propose that the P- and L-rings form around the assembled rod (35–37).

If the FOMC is not an assembly intermediate, it may be a residual structure left after a flagellum detaches. We measured the position of FOMCs relative to the cell pole and found that most were within 60 nm of the pole, with a distribution that matched that of intact flagellar motors in both WT and Δ*fleN* cells (see Fig. S7A and B in the supplemental material). This overlapping distribution is consistent with FOMCs being residual structures generated from flagellar motors, as the only known signal for polar flagellar placement is provided by the cytoplasmic protein FlhF (38). FOMCs were much more common in Δ*fleN* bacteria than in WT cells, accounting for 32% of all analyzed structures in Δ*fleN* cells (566/1747) compared with 5.5% in WT PAK (6/109) (Table 1). We examined WT and Δ*fleN* cells for evidence of increased flagellar loss in mutant bacteria and observed many detached flagellar filaments in samples of Δ*fleN* bacteria (Fig. 5). In contrast, detached flagella were rarely seen in samples prepared from WT bacteria, which is consistent with the rare observation of FOMCs in these cells.

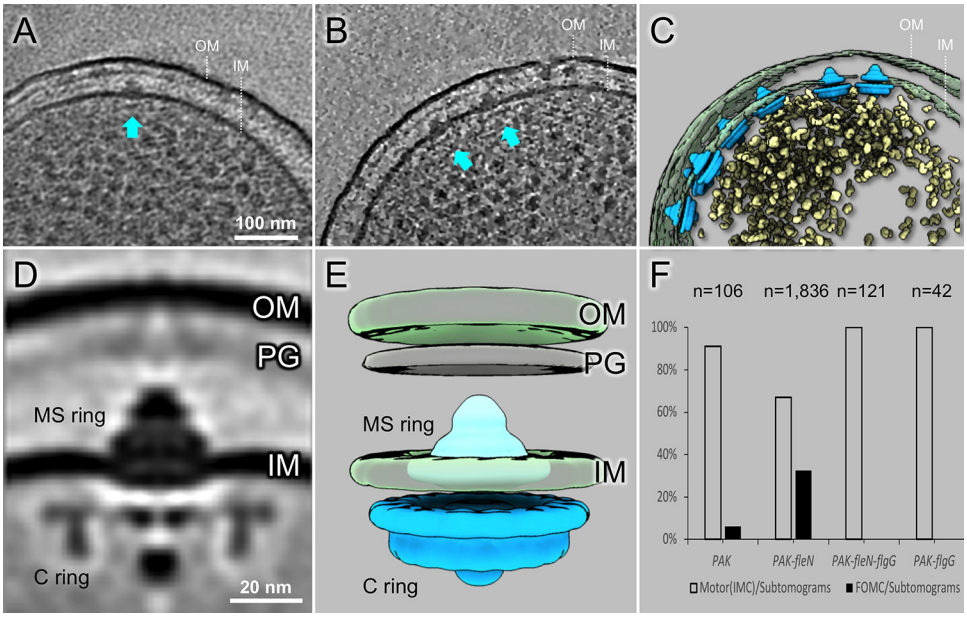

FIG 4 *P. aeruginosa* Δ*flgG* and Δ*fleN* Δ*flgG* fail to assemble FOMCs. (A) A representative slice from a Δ*flgG* tomogram shows the MS/C-rings (arrow). (B) A representative slice from a Δ*fleN* Δ*flgG* tomogram shows two MS/C-rings (arrows). (C) A surface view of the tomogram in (B) shows seven MS/C-rings. (D) A central section from the averaged structure of the MS/C-rings. The distal rod is absent, while both MS/C-rings and expert apparatus are clearly resolved. (E) A surface view of the averaged structure shows the MS-ring (colored in cyan) embedded in inner membrane (IM) and the C-ring in blue. (F) Number of motors (or MS/C-rings) and FOMC observed in different strains. White bars represent motors (MS-ring and C-ring) found in cells; black bars indicate FOMCs. No FOMCs were seen in Δ*flgG* and Δ*fleN* Δ*flgG* cells.

DISCUSSION

Flagella are the principal organelles powering motility in many bacterial species. These organelles share a conserved core structure but also demonstrate marked structural variation that is thought to underlie the ability of bacteria to swim through a wide range of environments (5, 6). We have used cryo-ET to visualize polar flagella in *P. aeruginosa* and lateral flagella in *S.* Typhimurium, revealing notable differences between these two flagellar systems. Specifically, the polar flagellum of *P. aeruginosa* possesses additional T- and H-rings that assemble outside the P- and L-rings, respec-

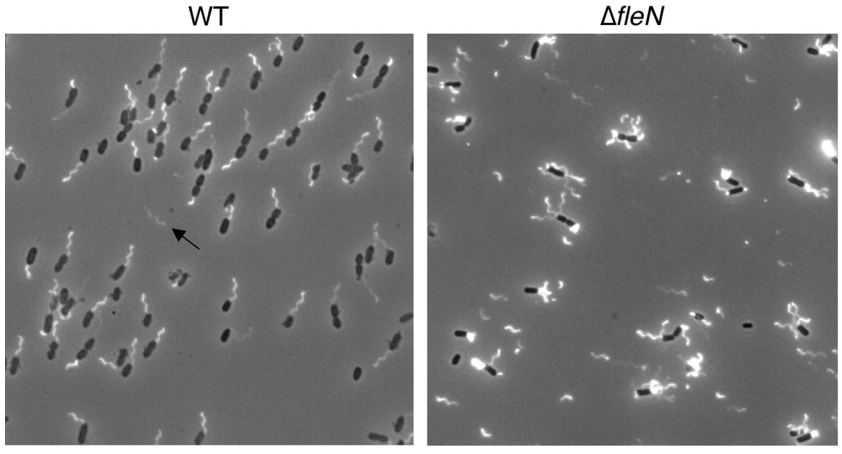

FIG 5 Detached flagella are frequently seen for Δ*fleN* bacteria. Live *P. aeruginosa* WT and Δ*fleN* bacteria expressing *fliC*(*T394C*) were stained with Alexa Fluor 488-maleimide and visualized by fluorescence microscopy. Single polar flagella are clearly visible on most WT cells, and one detached flagellum is indicated by an arrow. Δ*fleN* cells show multiple polar flagella, and many detached flagellar filaments are observed.

tively. This wider stator would allow the *P. aeruginosa* motor to generate a greater maximum torque than *S.* Typhimurium (15), allowing *P. aeruginosa* to swim at higher velocities and swarm through more viscous media, as observed recently (39).

MotY is likely involved in the formation of the T-ring, as *motY* mutants lack this feature in both *P. aeruginosa* and *V. alginolyticus* (31). The protein(s) responsible for H-ring formation remains unknown. However, the H-ring proteins likely cause the marked deflection of the outer membrane seen at the motor-membrane interface (Fig. S2), which distinguishes the *P. aeruginosa* flagellum from those of *V. alginolyticus* and *S.* Typhimurium.

Kaplan et al. recently used cryo-ET to examine the polar motors of *Shewanella oneidensis*, *Legionella pneumophila*, and *P. aeruginosa* (16). The structure that they present for the *P. aeruginosa* motor lacks the H-ring-like densities that we clearly observe in both the complete flagellar motor and the FOMC and instead resembles the low-pass filtered structure shown in Fig. S3D. This difference in resolution between their structure and ours may account for the additional structures and detail that we observe; it is also possible that their use of a different *P. aeruginosa* strain (PAO1) grown overnight in minimal media contributes to these differences.

Flagellar gene expression in both *S.* Typhimurium and *P. aeruginosa* is tightly regulated and coupled to the completion of flagellar intermediates, with the transcription of genes encoding hook-basal body (HBB) components preceding transcription of the flagellar filament subunit, stator proteins, or chemotaxis receptors (19, 20). The "early" flagellar genes encoding HBB components are under the control of master regulators, such as FlhDC in *S.* Typhimurium and FleQ in *P. aeruginosa*, and are expressed at the same time (19, 20). The Sec-dependent assembly of the inner membrane MS-ring, with which the cytoplasmic C-ring and export apparatus associate, creates a flagellar type III secretion system responsible for secreting proximal and distal rod proteins, as well as subunits of the hook and filament. The rod passes through the peptidoglycan layer and outer membrane within P- and L-rings, respectively. FlgI and FlgH, the proteins that form the P- and L-rings, also use the Sec secretory pathway to reach the periplasmic space (40). In addition to forming an outer membrane "bushing" for flagellar rod rotation, the L-ring appears to catalyze removal of the FlgJ rod cap, allowing assembly of the hook cap protein FlgD and the transition to extracellular hook assembly (41). The long-accepted model of flagellar assembly proposes that P/L-rings form around a completed rod, with assembly of the L-ring catalyzing the removal of the FlgJ rod cap and coupling the formation of the outer membrane pore to the rod-to-hook transition (36, 37). We observed isolated FOMCs in both *S.* Typhimurium and *P. aeruginosa*, showing that the L/P-ring outer membrane plugged "pore" can stably exist in the absence of the flagellar inner membrane or rod components. We considered the possibility that the FOMCs are intermediates that assemble independently of the MS-ring, C-ring, and rod proteins. However, the absence of FOMCs in bacteria lacking FlgG provides compelling evidence that the FOMC cannot form in the absence of this distal rod protein. This is in contrast to the assembly of structurally related type 3 secretion systems, in which the outer membrane secretin pore can assemble independently and dock with the inner membrane rings (42).

FOMCs are likely to be remnants of flagella that have detached from the cell, although this process must be relatively uncommon under conditions of exponential growth, given the low frequency of these structures in WT *P. aeruginosa* cells (Fig. 6). A recent paper describes similar-appearing flagellar "relics" in *V. cholerae* and *Plesiomonas shigelloides* (43). The latter is a member of the family *Enterobacteriaceae* which is found in fresh or brackish waters and is associated with diarrheal disease following the consumption of raw oysters (44). *P. shigelloides* produces polar flagella when grown in liquid media and assembles lateral flagella when grown in solid or semisolid media (45). The polar flagellum of *Plesiomonas* (formerly *Aeromonas*) spp. is powered by Na^+-conducting stators (46) as is the case for marine *Vibrio* spp. The polar flagella of both *P. shigelloides* and *V. cholerae* are proposed to be ejected under conditions of nutrient deprivation, leaving numerous flagellar "relics" at the *P. shigelloides* pole (43). Reduced

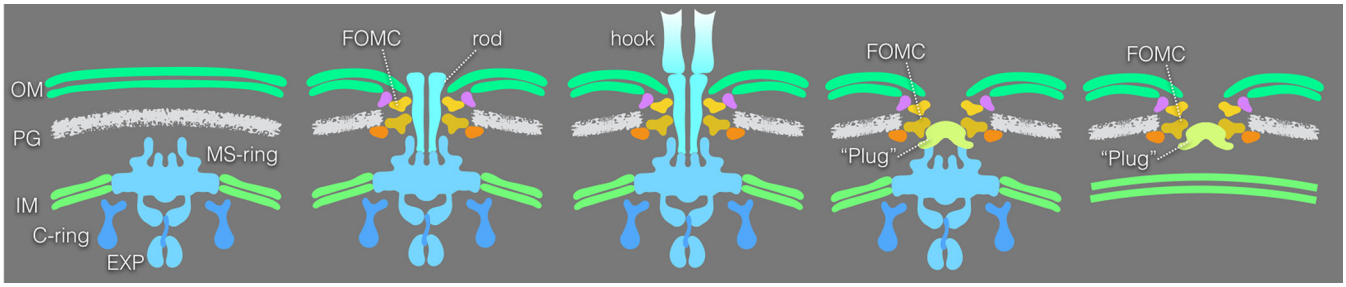

FIG 6 A schematic model of flagellar assembly. The first panel shows an early stage of flagellar assembly with the MS-ring in the inner membrane. The second panel shows a FOMC assembled around the rod. The third panel shows an intermediate transitioning from rod to hook assembly. The fourth panel shows a subcomplex lacking the rod and hook. The last panel shows an FOMC. The final two structures are likely products of flagellar disassembly. EXP, export apparatus; OM, outer membrane; IM, inner membrane; PG, peptidoglycan layer.

swimming speeds and decreased numbers of surface flagella are observed as *P. shigelloides* and *V. cholerae* enter stationary phase, while *S.* Typhimurium swimming speed and flagellar number increase with culture density. Although Ferreira et al. argue that *P. aeruginosa* must undergo a similar process of flagellar "ejection" based on their observation of flagellar relics in this species, no data supporting this hypothesis are presented in their study. Our results suggest that *P. aeruginosa* FOMCs result when flagella detach, as happens frequently in the Δ*fleN* mutant and rarely in WT *P. aeruginosa*. As many Δ*fleN* bacteria still possess multiple polar flagella at a time when both detached flagellar filaments (Fig. 5) and FOMCs (Fig. 2B) are also observed, we hypothesize that detachment and/or shearing of entangled flagella is more likely to account for our findings than programmed flagellar ejection. Similar mechanical loss may also lead to the rare FOMCs that we observed for *S.* Typhimurium.

In summary, we have used cryo-ET to observe *in situ* structures associated with the assembly of *P. aeruginosa* and *S.* Typhimurium flagella. These *in situ* structures have revealed the features of the *P. aeruginosa* polar flagellar motor in unprecedented detail. Our work has also demonstrated that MotY contributes to the formation of the T-ring in *P. aeruginosa*, but additional components that form the "H-ring" structure of this envelope spanning nanomachine still await discovery.

MATERIALS AND METHODS

Bacterial strains and plasmids. Bacterial strains used in this study are listed in Table 2. *P. aeruginosa*, *E. coli*, and *S.* Typhimurium strains were cultured in Luria broth (LB) with shaking at 37°C unless otherwise indicated. The following antibiotics were added as indicated: chloramphenicol (12.5 μg/ml) and gentamicin (15 μg/ml, *E. coli*; 100 μg/ml, *P. aeruginosa*).

Strain construction. All PCR primers used in this study are listed in Table 3 and were synthesized by the Keck Facility (Yale University). Unmarked, in-frame deletion of *P. aeruginosa* genes was carried out by allelic exchange (47). Briefly, ~1-kb regions upstream and downstream of *fleN*, *flgG*, or *motY* were PCR amplified from WT genomic DNA with Phusion polymerase (New England BioLabs [NEB]) using gene-specific N1/N2 and C1/C2 primer pairs and then spliced by overlap extension using primers N1/C2. The resulting fragment was integrated into a Gateway-adapted pEX-based deletion vector and confirmed by Sanger sequencing. The pEX-knockout (KO) plasmid was transformed into chemically competent *E. coli* S17.1 and then mated into *P. aeruginosa*. Exconjugant merodiploids were selected on Vogel-Bonner medium (VBM)-gentamicin and then plated on VBM and 10% (wt/vol) sucrose to select for excision of plasmid backbone sequences. Knockout candidates were screened by PCR and confirmed by motility phenotype and microscopy.

The flagellin-encoding gene *fliC* was mutated to replace threonine with cysteine at amino acid position 394 to allow staining of flagellar filaments in live, unfixed cells with Alexa Fluor 488 C_5 maleimide, as previously described (48). Gene-specific N1/N2 and C1/C2 primer pairs incorporating the mutation were used to PCR amplify *fliC* from PA14; these amplicons were spliced by overlap extension using primers N1/C2 and integrated into pDONRX. This construct was confirmed by Sanger sequencing and then employed as described above to replace the WT *fliC* genes of PA14 and PA14 Δ*fleN*.

The full-length *flgG* gene was PCR amplified from WT genomic DNA using Phusion polymerase (NEB) and cloned into pMQ72 (49) under the control of an arabinose-inducible pBAD promoter.

Swimming assays. Two microliters of an exponential-phase bacterial culture was spotted onto LB solidified with 0.3% agar and incubated overnight at 30°C. Antibiotics and arabinose (0.2%) were added to plates carrying pMQ72 vectors.

TABLE 2 Bacterial strains and plasmids used in this study

Strain or plasmid	Genotype or description[a]	Reference or source
Strains		
P. aeruginosa		
PAK	WT	60
PAK Δ*fleN*	Unmarked, in-frame deletion of *fleN*	This study
PAK Δ*flgG*	Unmarked, in-frame deletion of *flgG*	This study
PAK Δ*fleN* Δ*flgG*	Unmarked, in-frame deletion of *fleN* and *flgG*	This study
PAK Δ*motY*	Unmarked, in-frame deletion of *motY*	This study
PA14	WT	61
PA14 *fliC*(*T394C*)	Replacement of chromosomal *fliC* in PA14	This study
PA14 Δ*fleN*	Unmarked, in-frame deletion of *fleN* in PA14	This study
PA14 *fliC*(*T394C*) Δ*fleN*	Replacement of chromosomal *fliC* in PA14 Δ*fleN*	This study
S. Typhimurium SB1780	*minD*::*cat* (Cm^r); minicell producer	51
E. coli		
DH5α		Invitrogen
S17.1	*thi pro hsdR recA* RP4-2 (Tc::Mu) (Km::Tn*7*)	62
Plasmids		
pEX-GW	pEX-based deletion vector, Gm^r	63
pEX-fleNKO	pDONRX with ~1-kb region upstream and downstream of *fleN*; Gm^r	This study
pEX-flgGKO	pDONRX with ~1-kb region upstream and downstream of *flgG*; Gm^r	This study
pEX-motYKO	pDONRX with ~1-kb region upstream and downstream of *motY*; Gm^r	This study
pMQ72	Expression vector, Gm^r	49
pMQ72-FlgG	Plasmid expressing FlgG under pBAD control, Gm^r	This study

[a]Cm^r, chloramphenicol resistant; Gm^r, gentamicin resistant.

Flagellar staining. Flagellar filaments were stained as previously described (48). Briefly, PA14 *fliC*(*T394C*) and PA14 Δ*fleN fliC*(*T394C*) bacteria were grown to log phase (optical density at 600 [OD_{600}], ~0.5) in LB at 37°C. One milliliter of cell culture was gently pelleted (5,000 × *g* for 5 min), washed once with phosphate-buffered saline (PBS; pH 8), resuspended in 50 μl of PBS containing 50 μg/ml Alexa Fluor 488 C_5 maleimide (Thermo Fisher Scientific), and incubated for 3 min at room temperature. Cells were washed with PBS and resuspended in 30 μl of PBS. Four microliters of suspension was spotted to a clean microscope slide, immobilized with a poly-L-lysine-treated coverslip, and imaged using a Nikon Eclipse Ti-E inverted microscope equipped with an Andor Zyla 5.5MP 10-tap scientific complementary metal-oxide semiconductor (sCMOS) camera.

Sample preparation for cryo-ET. Two microliters of an overnight *P. aeruginosa* LB culture (grown at 37°C with shaking) was spotted onto a 1% LB agar plate and incubated for 12 hours at 37°C. The cells at the edges of colonies were collected and checked for motility. Collected cells were then washed once with PBS buffer and resuspended. Colloidal gold particles (10 nm) were added to the cell suspension to yield a 10× dilution and then deposited on a freshly glow-discharged, holey carbon grid (copper 200 mesh; Quantifoil) for 1 min. The grid with a 5-μl mixture was blotted with filter paper (Waterman

TABLE 3 Primers

Name	Sequence (5′ to 3′)
fleN N1	GGGGACAAGTTTGTACAAAAAAGCAGGCTTGGCGCATGCTGTTGGCGCACCTGT
fleN N2	CCGCTGTCATACGGCCGAACCACCCATCTGCTTCATACCTTG
fleN C1	CAAGGTATGAAGCAGATGGGTGGTTCGGCCGTATGACAGCGG
fleN C2	GGGGACCACTTTGTACAAGAAAGCTGGGTTCTTGTCCAAGTAAACCTCCGTACAGA
flgG N1	GGGGACAAGTTTGTACAAAAAAGCAGGCTGGAGGATTCGATGGACAAGAT
flgG N2	GACGAAGGACTTGCTGACCCACAGTGCCG
flgG C1	GTCAGCAAGTCCTTCGTCACCCAGAATCTTTG
flgG C2	GGGGACCACTTTGTACAAGAAAGCTGGGTGGATGCTGGCGATATCCTTCA
motY N1	GGGGACAAGTTTGTACAAAAAAGCAGGCTCCGAGTCGGTGCCGAGGAAGA
motY N2	CGCGACTCAAACCGTGGGTTTAAGGCGCGGCTGCACGACGGC
motY C1	GCCGTCGTGCAGCCGCGCCTTAAACCCACGGTTTGAGTCGCG
motY C2	GGGGACCACTTTGTACAAGAAAGCTGGGTCAGCTCGATGTAGGTCGGGGT
fliC(T394C) N1	GGGGACAAGTTTGTACAAAAAAGCAGGCTGCGACCTGGCCCTGCAATC
fliC(T394C) N2	CGCCGTCTGCGCAGGAGATGTCGACGCTGGCAAC
fliC(T394C) C1	CATCTCCTGCGCAGACGGCGCCCAGAACGCCA
fliC(T394C) C2	GGGGACCACTTTGTACAAGAAAGCTGGGTCTTCGATAGGGCAAGCACCATG
EcoRI-flgG	GGAGAATCCTTGCAAATCAGCTAATCACTTGAG
flgG-HindIII	GGACAAGCTTCTACCTCGCGGCGTACA

qualitative filter paper, grade 1) and rapidly plunge-frozen in liquid ethane using a gravity-driven plunger apparatus, as described previously (31, 50).

S. Typhimurium SB1780 was grown overnight at 37°C in LB containing 0.3 M NaCl. Bacterial subcultures were prepared the following day and enriched for minicells, as previously described (51). Minicell deposition and freezing were carried out as described above for *P. aeruginosa*.

Cryo-ET data collection and image processing. The data from *P. aeruginosa* PAK Δ*fleN* and *S.* Typhimurium were collected using a Polara G2 electron microscope (FEI). The data from *P. aeruginosa* WT cells were collected using a Titan Krios electron microscope (Thermo Fisher Scientific). Both microscopes were equipped with a 300-kV field emission gun and a direct electron detector (Gatan K2 Summit). Images collected by the Polara G2 electron microscope were observed at ×15,000 magnification and at 4- to 6-μm defocus, resulting in 0.25 nm/pixel. The images taken by the Titan Krios electron microscope were collected at focus using a Volta phase plate and energy filter with a 20-eV slit. The resulting physical resolution is 0.27 nm/pixel. All data were acquired with SerialEM software (52). A total dose of 50 $e^{-}/Å^2$ is distributed among 35 tilt images covering angles from −51° to +51° at tilt steps of 3° and starting to collect tilts series at −30°. For every single tilt series collection, the dose-fractionated mode was used to generate 8 to 10 frames per projection image. Collected dose-fractionated data were first subjected to the motion correction program to generate drift-corrected stack files (53). The stack files were aligned using gold fiducial markers and volumes reconstructed by the weighted back-projection method, using Tomoauto (54), IMOD (55), and Tomo3d (56).

Subtomogram analysis with i3 package. Bacterial flagellar motors were detected manually and analyzed using the i3 program (57, 58). In total, 1,746 subtomograms of *P. aeruginosa* motors from PAK Δ*fleN* and 3,695 subtomograms of *S.* Typhimurium motors from SB1780 were used for subtomogram analysis. The i3 tomographic package was used on the basis of the "alignment by classification" method with missing wedge compensation for generating the averaged structure of the motor, as described previously (58). Detailed information about tomograms and subtomograms in this study is provided in Table 1.

Three-dimensional visualization. Tomographic reconstructions were visualized using IMOD (55). The segmentation was generated using IMOD and surface rendering was done with UCSF chimera (59).

Determination of flagellar motor and FOMC distance from the *P. aeruginosa* cell pole. The distance of motors and FOMCs from the cell pole was extracted from tomograms for 38 motors and 29 FOMCs in Δ*fleN* cells and for 103 motors and 6 FOMCs in WT PAK cells, and data were plotted using Microsoft Excel.

SUPPLEMENTAL MATERIAL

Supplemental material for this article may be found at https://doi.org/10.1128/JB.00117-19.

SUPPLEMENTAL FILE 1, PDF file, 3.2 MB.

ACKNOWLEDGMENTS

This work was supported by grants GM107629 and R01AI087946 (to J.L.), AI075051 and AI117333 (to B.I.K.), and AI079022 (to J.E.G.) from National Institutes of Health.

REFERENCES

1. Minamino T, Imada K. 2015. The bacterial flagellar motor and its structural diversity. Trends Microbiol 23:267–274. https://doi.org/10.1016/j.tim.2014.12.011.
2. Minamino T, Macnab RM. 1999. Components of the *Salmonella* flagellar export apparatus and classification of export substrates. J Bacteriol 181:1388–1394.
3. Jones CJ, Homma M, Macnab RM. 1987. Identification of proteins of the outer (L and P) rings of the flagellar basal body of *Escherichia coli*. J Bacteriol 169:1489–1492. https://doi.org/10.1128/jb.169.4.1489-1492.1987.
4. Jones CJ, Homma M, Macnab RM. 1989. L-, P-, and M-ring proteins of the flagellar basal body of *Salmonella typhimurium*: gene sequences and deduced protein sequences. J Bacteriol 171:3890–3900. https://doi.org/10.1128/jb.171.7.3890-3900.1989.
5. Chen S, Beeby M, Murphy GE, Leadbetter JR, Hendrixson DR, Briegel A, Li Z, Shi J, Tocheva EI, Muller A, Dobro MJ, Jensen GJ. 2011. Structural diversity of bacterial flagellar motors. EMBO J 30:2972–2981. https://doi.org/10.1038/emboj.2011.186.
6. Zhao X, Norris SJ, Liu J. 2014. Molecular architecture of the bacterial flagellar motor in cells. Biochemistry 53:4323–4333. https://doi.org/10.1021/bi500059y.
7. Chaban B, Hughes HV, Beeby M. 2015. The flagellum in bacterial pathogens: for motility and a whole lot more. Semin Cell Dev Biol 46:91–103. https://doi.org/10.1016/j.semcdb.2015.10.032.
8. Wadhams GH, Armitage JP. 2004. Making sense of it all: bacterial chemotaxis. Nat Rev Mol Cell Biol 5:1024–1037. https://doi.org/10.1038/nrm1524.
9. McCarter L. 2004. Dual flagellar systems enable motility under different circumstances. J Mol Microbiol Biotechnol 7:18–29. https://doi.org/10.1159/000077866.
10. Sato K, Homma M. 2000. Functional reconstitution of the Na(+)-driven polar flagellar motor component of *Vibrio alginolyticus*. J Biol Chem 275:5718–5722. https://doi.org/10.1074/jbc.275.8.5718.
11. Atsumi T, McCarter L, Imae Y. 1992. Polar and lateral flagellar motors of marine *Vibrio* are driven by different ion-motive forces. Nature 355:182–184. https://doi.org/10.1038/355182a0.
12. Charon NW, Cockburn A, Li C, Liu J, Miller KA, Miller MR, Motaleb MA, Wolgemuth CW. 2012. The unique paradigm of spirochete motility and chemotaxis. Annu Rev Microbiol 66:349–370. https://doi.org/10.1146/annurev-micro-092611-150145.
13. Liu R, Ochman H. 2007. Origins of flagellar gene operons and secondary flagellar systems. J Bacteriol 189:7098–8104. https://doi.org/10.1128/JB.00643-07.
14. Pallen MJ, Penn CW, Chaudhuri RR. 2005. Bacterial flagellar diversity in the post-genomic era. Trends Microbiol 13:143–149. https://doi.org/10.1016/j.tim.2005.02.008.
15. Beeby M, Ribardo DA, Brennan CA, Ruby EG, Jensen GJ, Hendrixson DR. 2016. Diverse high-torque bacterial flagellar motors assemble wider stator rings using a conserved protein scaffold. Proc Natl Acad Sci U S A 113:E1917–E1926. https://doi.org/10.1073/pnas.1518952113.
16. Kaplan M, Ghosal D, Subramanian P, Oikonomou CM, Kjaer A, Pirbadian S, Ortega DR, Briegel A, El-Naggar MY, Jensen GJ. 2019. The presence

and absence of periplasmic rings in bacterial flagellar motors correlates with stator type. Elife 8:e43487. https://doi.org/10.7554/eLife.43487.
17. Cai Q, Li Z, Ouyang Q, Luo C, Gordon VD. 2016. Singly flagellated *Pseudomonas aeruginosa* chemotaxes efficiently by unbiased motor regulation. mBio 7:e00013. https://doi.org/10.1128/mBio.00013-16.
18. Xie L, Altindal T, Chattopadhyay S, Wu XL. 2011. Bacterial flagellum as a propeller and as a rudder for efficient chemotaxis. Proc Natl Acad Sci U S A 108:2246–2251. https://doi.org/10.1073/pnas.1011953108.
19. Dasgupta N, Wolfgang MC, Goodman AL, Arora SK, Jyot J, Lory S, Ramphal R. 2003. A four-tiered transcriptional regulatory circuit controls flagellar biogenesis in *Pseudomonas aeruginosa*. Mol Microbiol 50:809–824. https://doi.org/10.1046/j.1365-2958.2003.03740.x.
20. Chevance FF, Hughes KT. 2017. Coupling of flagellar gene expression with assembly in *Salmonella enterica*. Methods Mol Biol 1593:47–71. https://doi.org/10.1007/978-1-4939-6927-2_4.
21. Doyle TB, Hawkins AC, McCarter L. 2004. The complex flagellar torque generator of *Pseudomonas aeruginosa*. J Bacteriol 186:6341–6350. https://doi.org/10.1128/JB.186.19.6341-6350.2004.
22. Kuchma SL, Delalez NJ, Filkins LM, Snavely EA, Armitage JP, O'Toole GA. 2015. Cyclic di-GMP-mediated repression of swarming motility by *Pseudomonas aeruginosa* PA14 requires the MotAB stator. J Bacteriol 197:420–430. https://doi.org/10.1128/JB.02130-14.
23. Ortega DR, Fleetwood AD, Krell T, Harwood CS, Jensen GJ, Zhulin IB. 2017. Assigning chemoreceptors to chemosensory pathways in *Pseudomonas aeruginosa*. Proc Natl Acad Sci U S A 114:12809–12814. https://doi.org/10.1073/pnas.1708842114.
24. Conrad JC, Gibiansky ML, Jin F, Gordon VD, Motto DA, Mathewson MA, Stopka WG, Zelasko DC, Shrout JD, Wong GC. 2011. Flagella and pili-mediated near-surface single-cell motility mechanisms in *P. aeruginosa*. Biophys J 100:1608–1616. https://doi.org/10.1016/j.bpj.2011.02.020.
25. O'Toole GA, Kolter R. 1998. Flagellar and twitching motility are necessary for *Pseudomonas aeruginosa* biofilm development. Mol Microbiol 30:295–304. https://doi.org/10.1046/j.1365-2958.1998.01062.x.
26. Dasgupta N, Arora SK, Ramphal R. 2000. *fleN*, a gene that regulates flagellar number in *Pseudomonas aeruginosa*. J Bacteriol 182:357–364. https://doi.org/10.1128/JB.182.2.357-364.2000.
27. Dasgupta N, Ramphal R. 2001. Interaction of the antiactivator FleN with the transcriptional activator FleQ regulates flagellar number in *Pseudomonas aeruginosa*. J Bacteriol 183:6636–6644. https://doi.org/10.1128/JB.183.22.6636-6644.2001.
28. Correa NE, Peng F, Klose KE. 2005. Roles of the regulatory proteins FlhF and FlhG in the *Vibrio cholerae* flagellar transcription hierarchy. J Bacteriol 187:6324–6332. https://doi.org/10.1128/JB.187.18.6324-6332.2005.
29. Kusumoto A, Kamisaka K, Yakushi T, Terashima H, Shinohara A, Homma M. 2006. Regulation of polar flagellar number by the flhF and flhG genes in *Vibrio alginolyticus*. J Biochem 139:113–121. https://doi.org/10.1093/jb/mvj010.
30. Schuhmacher JS, Rossmann F, Dempwolff F, Knauer C, Altegoer F, Steinchen W, Dorrich AK, Klingl A, Stephan M, Linne U, Thormann KM, Bange G. 2015. MinD-like ATPase FlhG effects location and number of bacterial flagella during C-ring assembly. Proc Natl Acad Sci U S A 112:3092–3097. https://doi.org/10.1073/pnas.1419388112.
31. Zhu S, Nishikino T, Hu B, Kojima S, Homma M, Liu J. 2017. Molecular architecture of the sheathed polar flagellum in *Vibrio alginolyticus*. Proc Natl Acad Sci U S A 114:10966–10971. https://doi.org/10.1073/pnas.1712489114.
32. Terashima H, Koike M, Kojima S, Homma M. 2010. The flagellar basal body-associated protein FlgT is essential for a novel ring structure in the sodium-driven Vibrio motor. J Bacteriol 192:5609–5615. https://doi.org/10.1128/JB.00720-10.
33. Zhu S, Nishikino T, Kojima S, Homma M, Liu J. 2018. The Vibrio H-ring facilitates the outer membrane penetration of the polar sheathed flagellum. J Bacteriol 200:e00387-18. https://doi.org/10.1128/JB.00387-18.
34. Fujii T, Kato T, Hiraoka KD, Miyata T, Minamino T, Chevance FF, Hughes KT, Namba K. 2017. Identical folds used for distinct mechanical functions of the bacterial flagellar rod and hook. Nat Commun 8:14276. https://doi.org/10.1038/ncomms14276.
35. Kubori T, Shimamoto N, Yamaguchi S, Namba K, Aizawa S. 1992. Morphological pathway of flagellar assembly in *Salmonella typhimurium*. J Mol Biol 226:433–446. https://doi.org/10.1016/0022-2836(92)90958-M.
36. Macnab RM. 2003. How bacteria assemble flagella. Annu Rev Microbiol 57:77–100. https://doi.org/10.1146/annurev.micro.57.030502.090832.
37. Chevance FF, Hughes KT. 2008. Coordinating assembly of a bacterial macromolecular machine. Nat Rev Microbiol 6:455–465. https://doi.org/10.1038/nrmicro1887.
38. Murray TS, Kazmierczak BI. 2006. FlhF is required for swimming and swarming in *Pseudomonas aeruginosa*. J Bacteriol 188:6995–7004. https://doi.org/10.1128/JB.00790-06.
39. Schniederberend M, Johnston JF, Shine E, Shen C, Jain R, Emonet T, Kazmierczak BI. 2019. Modulation of flagellar rotation in surface-attached bacteria: a circuit for rapid surface-sensing. bioRxiv https://doi.org/10.1101/567438.
40. Karlinsey JE, Pease AJ, Winkler ME, Bailey JL, Hughes KT. 1997. The flk gene of *Salmonella typhimurium* couples flagellar P- and L-ring assembly to flagellar morphogenesis. J Bacteriol 179:2389–2400. https://doi.org/10.1128/jb.179.7.2389-2400.1997.
41. Cohen EJ, Hughes KT. 2014. Rod-to-hook transition for extracellular flagellum assembly is catalyzed by the L-ring-dependent rod scaffold removal. J Bacteriol 196:2387–2395. https://doi.org/10.1128/JB.01580-14.
42. Galan JE, Lara-Tejero M, Marlovits TC, Wagner S. 2014. Bacterial type III secretion systems: specialized nanomachines for protein delivery into target cells. Annu Rev Microbiol 68:415–438. https://doi.org/10.1146/annurev-micro-092412-155725.
43. Ferreira JL, Gao FZ, Rossmann FM, Nans A, Brenzinger S, Hosseini R, Wilson A, Briegel A, Thormann KM, Rosenthal PB, Beeby M. 2019. Gamma-proteobacteria eject their polar flagella under nutrient depletion, retaining flagellar motor relic structures. PLoS Biol 17:e3000165. https://doi.org/10.1371/journal.pbio.3000165.
44. Chen X, Chen Y, Yang Q, Kong H, Yu F, Han D, Zheng S, Cui D, Li L. 2013. *Plesiomonas shigelloides* infection in Southeast China. PLoS One 8:e77877. https://doi.org/10.1371/journal.pone.0077877.
45. Merino S, Aquilini E, Fulton KM, Twine SM, Tomas JM. 2015. The polar and lateral flagella from *Plesiomonas shigelloides* are glycosylated with legionaminic acid. Front Microbiol 6:649. https://doi.org/10.3389/fmicb.2015.00649.
46. Wilhelms M, Vilches S, Molero R, Shaw JG, Tomas JM, Merino S. 2009. Two redundant sodium-driven stator motor proteins are involved in *Aeromonas hydrophila* polar flagellum rotation. J Bacteriol 191:2206–2217. https://doi.org/10.1128/JB.01526-08.
47. Hoang TT, Karkhoff-Schweizer RR, Kutchma AJ, Schweizer HP. 1998. A broad-host-range Flp-FRT recombination system for site-specific excision of chromosomally-located DNA sequences: application for isolation of unmarked *Pseudomonas aeruginosa* mutants. Gene 212:77–86. https://doi.org/10.1016/S0378-1119(98)00130-9.
48. Blair KM, Turner L, Winkelman JT, Berg HC, Kearns DB. 2008. A molecular clutch disables flagella in the Bacillus subtilis biofilm. Science 320:1636–1638. https://doi.org/10.1126/science.1157877.
49. Shanks RM, Caiazza NC, Hinsa SM, Toutain CM, O'Toole GA. 2006. Saccharomyces cerevisiae-based molecular tool kit for manipulation of genes from gram-negative bacteria. Appl Environ Microbiol 72:5027–5036. https://doi.org/10.1128/AEM.00682-06.
50. Hu B, Morado DR, Margolin W, Rohde JR, Arizmendi O, Picking WL, Picking WD, Liu J. 2015. Visualization of the type III secretion sorting platform of *Shigella flexneri*. Proc Natl Acad Sci U S A 112:1047–1052. https://doi.org/10.1073/pnas.1411610112.
51. Hu B, Lara-Tejero M, Kong Q, Galán JE, Liu J. 2017. In situ molecular architecture of the *Salmonella* type III secretion machine. Cell 168:1065–1067. https://doi.org/10.1016/j.cell.2017.02.022.
52. Mastronarde DN. 2005. Automated electron microscope tomography using robust prediction of specimen movements. J Struct Biol 152:36–51. https://doi.org/10.1016/j.jsb.2005.07.007.
53. Li X, Mooney P, Zheng S, Booth CR, Braunfeld MB, Gubbens S, Agard DA, Cheng Y. 2013. Electron counting and beam-induced motion correction enable near-atomic-resolution single-particle cryo-EM. Nat Methods 10:584–590. https://doi.org/10.1038/nmeth.2472.
54. Morado DR, Hu B, Liu J. 2016. Using Tomoauto: a protocol for high-throughput automated cryo-electron tomography. J Vis Exp 107:e53608. https://doi.org/10.3791/53608.
55. Kremer JR, Mastronarde DN, McIntosh JR. 1996. Computer visualization of three-dimensional image data using IMOD. J Struct Biol 116:71–76. https://doi.org/10.1006/jsbi.1996.0013.
56. Agulleiro JI, Fernandez JJ. 2015. Tomo3D 2.0–exploitation of advanced vector extensions (AVX) for 3D reconstruction. J Struct Biol 189:147–152. https://doi.org/10.1016/j.jsb.2014.11.009.
57. Winkler H. 2007. 3D reconstruction and processing of volumetric data in cryo-electron tomography. J Struct Biol 157:126–137. https://doi.org/10.1016/j.jsb.2006.07.014.

58. Winkler H, Zhu P, Liu J, Ye F, Roux KH, Taylor KA. 2009. Tomographic subvolume alignment and subvolume classification applied to myosin V and SIV envelope spikes. J Struct Biol 165:64–77. https://doi.org/10.1016/j.jsb.2008.10.004.
59. Pettersen EF, Goddard TD, Huang CC, Couch GS, Greenblatt DM, Meng EC, Ferrin TE. 2004. UCSF Chimera—a visualization system for exploratory research and analysis. J Comput Chem 25:1605–1612. https://doi.org/10.1002/jcc.20084.
60. Frost LS, Paranchych W. 1977. Composition and molecular weight of pili purified from *Pseudomonas aeruginosa* K. J Bacteriol 131:259–269.
61. Rahme LG, Stevens EJ, Wolfort SF, Shao J, Tompkins RG, Ausubel FM. 1995. Common virulence factors for bacterial pathogenicity in plants and animals. Science 268:1899–1902. https://doi.org/10.1126/science.7604262.
62. Simon R, Priefer U, Puhler A. 1983. A broad host range mobilization system for in vivo genetic engineering: transposon mutagenesis in Gram negative bacteria. Nat Biotechnol 1:784–791. https://doi.org/10.1038/nbt1183-784.
63. Fulcher NB, Holliday PM, Klem E, Cann MJ, Wolfgang MC. 2010. The *Pseudomonas aeruginosa* Chp chemosensory system regulates intracellular cAMP levels by modulating adenylate cyclase activity. Mol Microbiol 76:889–904. https://doi.org/10.1111/j.1365-2958.2010.07135.x.